Journal of Computational Physics 420 (2020) 109705

Contents lists available at ScienceDirect

Journal of Computational Physics

www.elsevier.com/locate/jcp

Short note

A cancellation problem in hybrid particle-in-cell schemes due to finite particle size

A. Stanier *, L. Chacón, A. Le

Applied Mathematics and Plasma Physics, Los Alamos National Laboratory, Los Alamos, NM 87545, United States

ARTICLE INFO

Article history:
Received 13 December 2019
Received in revised form 5 May 2020
Accepted 2 July 2020
Available online 15 July 2020

Keywords:
Hybrid
Particle-in-cell
Plasma
Asymptotic-preserving
Cancellation problem
Space weather

ABSTRACT

The quasi-neutral hybrid particle-in-cell algorithm with kinetic ions and fluid electrons is a popular model to study multi-scale problems in laboratory, space, and astrophysical plasmas. Here, it is shown that the different spatial discretizations of ions as finite-spatial-size particles and electrons as a grid-based fluid can lead to significant numerical wave dispersion errors in the long wavelength limit ($kd_i \ll 1$, where k is the wavenumber and d_i is the ion skin-depth). The problem occurs when high-order particle-grid interpolations, or grid-based smoothing, spreads the electric field experienced by the ions across multiple spatial cells and leads to inexact cancellation of electric field terms in the total (ion + electron) momentum equation. Practical requirements on the mesh spacing $\Delta x/d_i$ are suggested to bound these errors from above. The accuracy impact of not respecting these resolution constraints is shown for a non-linear shock problem.

1. Introduction

Particle-in-cell (PIC) methods [1,2] are widely used to model kinetic plasma physics problems as they avoid the need to solve for the plasma distribution function on a 6D (3D-3V) grid, and they can be highly optimized to run on modern computer architectures with multiple levels of parallelism [3]. However, care must be taken as PIC simulations can potentially suffer from a number of algorithmic issues that are not commonly found in purely grid-based codes. Issues relate to statistical noise from the use of a finite number of macro-particles [4], and the numerical heating of these particles due to lack of discrete conservation properties [1,5]. To partially mitigate such effects, macro-particles are given finite spatial size to smooth the particle-grid interaction, and grid-based filtering can be applied to hydrodynamic moments and electromagnetic fields [1]. In PIC codes, these techniques are mostly beneficial in terms of stability and accuracy, provided that the physical signal of interest at a wavenumber k is not attenuated too much by this smoothing. The latter is ensured if the signal of interest is well resolved by the spatial grid: $k\Delta x \ll 1$, where Δx is the cell size.

The hybrid-PIC scheme differs from the fully kinetic PIC method in that the electrons are treated as a grid-based fluid [6–9]. This is done to enable the study of problems in which the coupling between macroscopic and ion kinetic scales is important [10–14], without the need to resolve stiff electron scales. However, algorithmic limitations in the hybrid-PIC approach have been less well studied than for fully kinetic PIC.

In this note, it is demonstrated that using high-order shape functions and/or grid-based smoothing can lead to a decrease in simulation accuracy if, in addition, the ion skin-depth is not adequately resolved. In this case, significant wave dispersion

* Corresponding author.
E-mail address: stanier@lanl.gov (A. Stanier).

https://doi.org/10.1016/j.jcp.2020.109705
0021-9991/

errors can occur in the long wavelength limit ($kd_i \ll 1$), even if the wave itself is well resolved by the numerical grid with $k\Delta x \ll 1$. The cause of the errors is the inexact cancellation of electric field terms when combining the ion and electron momentum equations to give a total momentum equation, as the electric field experienced by the ions is smoothed across multiple spatial cells. The numerical errors are avoided when using Nearest Grid Point (NGP) interpolation without smoothing. In this case, the electric field cancellation is exact, and the hybrid-PIC method is asymptotic preserving.

2. Hybrid-PIC algorithm

2.1. Continuum model

We consider the cold plasma kinetic-ion and fluid-electron quasi-neutral hybrid model. The kinetic ions are described by the distribution function $f_i = f_i(t, \boldsymbol{x}, \boldsymbol{v})$, which satisfies the Vlasov equation

$$\partial_t f_i + \boldsymbol{v} \cdot \nabla f_i + \frac{e}{m} (\boldsymbol{E} + \boldsymbol{v} \times \boldsymbol{B}) \cdot \nabla_v f_i = 0, \tag{1}$$

where e and m are the ion charge and mass. $\boldsymbol{E}(\boldsymbol{x}, t)$ is the electric field, which is given in the non-relativistic quasi-neutral limit via Ohm's law

$$\boldsymbol{E} = -\boldsymbol{u}_i \times \boldsymbol{B} + \frac{(\nabla \times \boldsymbol{B}) \times \boldsymbol{B}}{\mu_0 e n}, \tag{2}$$

and the magnetic field $\boldsymbol{B}$ is solved using Faraday's equation

$$\partial_t \boldsymbol{B} = -\nabla \times \boldsymbol{E}. \tag{3}$$

The system of equations is closed with the ion density (equal to the electron density by quasi-neutrality), n, and ion velocity, $\boldsymbol{u}_i$, which are calculated as moments of the distribution function

$$n = \int f_i d^3 v, \quad \boldsymbol{u}_i = \frac{1}{n} \int f_i \boldsymbol{v} d^3 v. \tag{4}$$

Before discussing how the cancellation problem arises in the discrete hybrid-PIC model, we review how the electric field terms cancel in the total momentum equation of the continuum model. Here, we use an equivalent moment description for the ions, which is closed due to the cold plasma assumption. The equations are also cast into dimensionless form where variables $\boldsymbol{\chi}$ are normalized by characteristic values $\boldsymbol{\chi}_0$, such that the dimensionless variables $\boldsymbol{\chi}/\boldsymbol{\chi}_0 \rightarrow \boldsymbol{\chi}$. The characteristic values are taken to be the magnetic field strength B_0, density n_0, ion mass m and charge e, Alfvén speed $v_0 = v_A = B_0/\sqrt{m\mu_0 n_0}$, electric field $E_0 = v_0 B_0$, length scale L_0, and time scale $t_0 = L_0/v_0$.

The normalized ion momentum equation is

$$\partial_t (n\boldsymbol{u}_i) + \nabla \cdot (n\boldsymbol{u}_i \boldsymbol{u}_i) = \frac{n}{\hat{d}_i} (\boldsymbol{E} + \boldsymbol{u}_i \times \boldsymbol{B}), \tag{5}$$

where $\hat{d}_i = d_i/L_0$, $d_i = v_A/\Omega_{ci}$ is the ion skin-depth, and $\Omega_{ci} = eB_0/m$ is the gyrofrequency. The normalized form of Ohm's law (2) is

$$\boldsymbol{E} = -\boldsymbol{u}_i \times \boldsymbol{B} + \frac{\hat{d}_i}{n} (\nabla \times \boldsymbol{B}) \times \boldsymbol{B}. \tag{6}$$

The total momentum equation is found by substituting the electric field from Eq. (6) into Eq. (5):

$$\partial_t (n\boldsymbol{u}_i) + \nabla \cdot (n\boldsymbol{u}_i \boldsymbol{u}_i) = (\nabla \times \boldsymbol{B}) \times \boldsymbol{B}. \tag{7}$$

Here, both the convective electric field terms of the form $\boldsymbol{u}_i \times \boldsymbol{B}$ and the factors of $\hat{d}_i/n$ exactly cancel, so that the total momentum equation has no explicit dependence on the normalized ion skin-depth, $\hat{d}_i$. However, as discussed below, this property of the continuum equations does not necessarily hold after spatial discretization.

Taking the long wavelength limit, $\hat{d}_i \rightarrow 0$, leaves Eq. (7) unchanged, and Ohm's law is given by the ideal magnetohydrodynamic form $\boldsymbol{E} = -\boldsymbol{u}_i \times \boldsymbol{B}$. However, it can be anticipated that if terms of the form $\boldsymbol{u}_i \times \boldsymbol{B}$ do not exactly cancel, there will be residual terms in the total momentum equation that will be proportional to $(1/\hat{d}_i)$. Taking $\hat{d}_i \rightarrow 0$ in this case will cause these residual terms to become singularly large. In the rest of this note, this cancellation problem is demonstrated analytically using the semi-discrete equations, and also numerically in both linear and non-linear examples.

2.2. Semi-discrete formulation

The above set of equations is spatially discretized using a PIC method for the ions, and a cell-centered finite difference method for the electron fluid. For simplicity, we treat only one spatial direction along the x-axis. The Vlasov equation (1) is solved by sampling the ion distribution function with macro-particle markers of weight w_p as $f_i(t,x,\boldsymbol{v}) \approx \sum_p w_p S_m(x - x_p(t))\delta(\boldsymbol{v} - \boldsymbol{v}_p(t))$. Here, the finite-size particle shape functions S_m are m-th order B-splines, which have compact support and form a partition of unity [1], and δ is the Dirac delta function. The markers are advanced using the normalized equations of motion

$$\frac{dx_p}{dt} = \boldsymbol{v}_p \cdot \hat{\boldsymbol{x}}, \tag{8}$$

$$\frac{d\boldsymbol{v}_p}{dt} = \frac{1}{\hat{d}_i}\left(\boldsymbol{E}_p + \boldsymbol{v}_p \times \boldsymbol{B}_p\right). \tag{9}$$

Grid-based quantities χ_g are defined at cell centers with cell index g, and derivatives are computed using second-order finite differences. Ohm's law (6) and Faraday's equation (3) are discretized as

$$\boldsymbol{E}_g = -\boldsymbol{u}_g \times \boldsymbol{B}_g + \frac{\hat{d}_i}{n_g}\left(\nabla_g \times \boldsymbol{B}_g\right) \times \boldsymbol{B}_g, \tag{10}$$

$$\partial_t \boldsymbol{B}_g = -\nabla_g \times \boldsymbol{E}_g, \tag{11}$$

where the 1D discrete curl operator is defined as $\nabla_g \times \boldsymbol{F}_g = \left[-\hat{\boldsymbol{y}}\left(F_{z,g+1} - F_{z,g-1}\right) + \hat{\boldsymbol{z}}\left(F_{y,g+1} - F_{y,g-1}\right)\right]/(2\Delta x)$.

The fluid moments gathered onto the grid cells are given by

$$n_g = \frac{1}{\Delta x}\mathrm{SM}_g\left(\sum_p w_p S_m(x_g - x_p)\right), \quad \boldsymbol{u}_g = \frac{1}{n_g \Delta x}\mathrm{SM}_g\left(\sum_p w_p S_m(x_g - x_p)\boldsymbol{v}_p\right). \tag{12}$$

Here $\mathrm{SM}_g(\chi_g) = (\chi_{g-1} + 2\chi_g + \chi_{g+1})/4$ is a binomial smoothing operator that acts on grid quantities. This kind of operator is often used in hybrid-PIC codes to reduce noise.

The electromagnetic fields are scattered from the grid cells to the particle positions as

$$\boldsymbol{E}_p = \sum_g S_m(x_g - x_p)\mathrm{SM}_g\left(\boldsymbol{E}_g\right), \quad \boldsymbol{B}_p = \sum_g S_m(x_g - x_p)\mathrm{SM}_g\left(\boldsymbol{B}_g\right). \tag{13}$$

2.3. Semi-discrete dispersion relation

In the following, a linear dispersion relation is calculated from the semi-discrete equations which demonstrates the source of the discrete cancellation errors. The predicted errors in the dispersion relation are then verified against numerical simulations. To simplify the analysis, we restrict the discussion to transverse electromagnetic waves propagating parallel to a uniform background magnetic field ($\boldsymbol{B_0} = B_0\hat{\boldsymbol{x}}$ with $B_0 = \text{const.}$) in a uniform ($n_0 = \text{const.}$), stationary ($\boldsymbol{E_0} = \boldsymbol{u_0} = \boldsymbol{0}$), and cold plasma. The ion particle phase-space coordinates $(x_p, \boldsymbol{v}_p)$ exist in continuous space. With the above assumptions, a cold ion momentum equation can be defined in the continuum [1]. Linearizing this equation about the specified equilibrium, and using the continuous space Fourier transform (Appendix A), gives

$$-i\omega\widetilde{\boldsymbol{\delta u}} = \frac{1}{\hat{d}_i}\left[\widetilde{\boldsymbol{\delta E}} + \widetilde{\boldsymbol{\delta u}} \times \boldsymbol{B}_0\right], \tag{14}$$

where $\widetilde{\delta\chi}$ are the Fourier mode amplitudes of the linear perturbations, existing in continuous space.

Equations (10)-(11) are defined on a spatial grid. Using the discrete Fourier transform (Appendix A) gives

$$\widetilde{\boldsymbol{\delta E}}_g = -\widetilde{\boldsymbol{\delta u}}_g \times \boldsymbol{B}_0 + \hat{d}_i(i\boldsymbol{\kappa} \times \widetilde{\boldsymbol{\delta B}_g}) \times \boldsymbol{B}_0, \tag{15}$$

$$-i\omega\widetilde{\boldsymbol{\delta B}}_g = -i\boldsymbol{\kappa} \times \widetilde{\boldsymbol{\delta E}}_g, \tag{16}$$

where $\boldsymbol{\kappa} = \hat{\boldsymbol{x}}[k\sin(k\Delta x)]/(k\Delta x)$ is the modification to the wavenumber from the finite-difference approximation of the nabla operator (Appendix A).

The transformed continuum electric field relates to the transformed discrete (grid) electric field as

$$\widetilde{\boldsymbol{\delta E}} = \mathrm{SM}(k\Delta x)S_m(-k\Delta x)\widetilde{\boldsymbol{\delta E}}_g, \tag{17}$$

where $\mathrm{SM}(k\Delta x) = \cos^2(k\Delta x/2)$, see Appendix A.

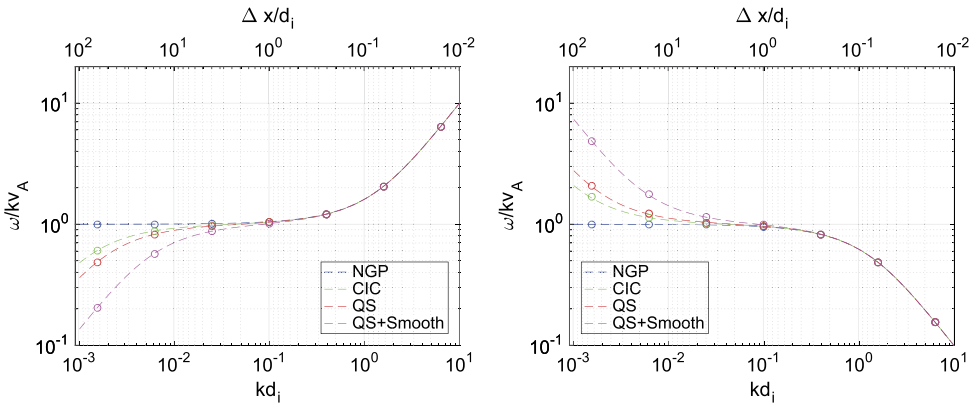

(a) Right-hand Alfvén-whistler (b) Left-hand Alfvén-cyclotron

Fig. 1. Semi-discrete dispersion relation from Eq. (20) shown as dashed curves for zeroth-order Nearest Grid Point (NGP, blue), first-order Cloud-In-Cell (CIC, green), second-order Quadratic-Spline (QS, red) without smoothing, and Quadratic-Spline with Binomial smoothing (QS+Smooth, magenta) applied to fields and moments. Circles are phase velocities measured from 1D electromagnetic hybrid simulations. Here, the wave is well resolved with fixed resolution $k\Delta x = \pi/32$ in each case, while kd_i is varied (bottom axis). The resolution $\Delta x/d_i$ (top axis) varies inversely proportional to kd_i in this case. Only NGP recovers the correct limits $\omega/kv_A \to 1$ as $kd_i \to 0$. (For interpretation of the colors in the figures, the reader is referred to the web version of this article.)

When sampling a quantity defined in the continuum onto a discrete mesh, it is necessary to account for aliasing effects. Following Chapter 8 of Ref. [1], the transformed discrete ion velocity moment relates to the transformed continuum moment as

$$\widetilde{\delta \boldsymbol{u}}_g = \mathrm{SM}(k\Delta x) \sum_q S_m(k_q \Delta x) \widetilde{\delta \boldsymbol{u}}(k_q), \tag{18}$$

where the sum is taken over the aliases $q \in \mathbb{Z}$ where $k_q = k - 2\pi q/\Delta x$. Eq. (14) can be written in terms of transformed grid-based quantities using Eqs. (17)-(18), as

$$-i\omega \widetilde{\delta \boldsymbol{u}}_g = \frac{1}{\hat{d}_i} |\mathrm{SM}(k\Delta x)|^2 \sum_q \left| S_m(k_q \Delta x) \right|^2 \widetilde{\delta \boldsymbol{E}}_g + \frac{1}{\hat{d}_i} \widetilde{\delta \boldsymbol{u}}_g \times \boldsymbol{B}_0, \tag{19}$$

where the periodicity in $2\pi q$ has been used for $\mathrm{SM}(k_q\Delta x) = \mathrm{SM}(k\Delta x)$ and $\widetilde{\delta \boldsymbol{E}}_g(k_q) = \widetilde{\delta \boldsymbol{E}}_g(k)$.

3. Hybrid cancellation problem

The resulting dispersion relation is found from Eqs. (15), (16), (19) as

$$\omega = \pm v_A \kappa \left(\sqrt{1 + \frac{1}{4}\left[d_i\kappa - \frac{1 - |\mathrm{SM}(k\Delta x)|^2 \sum_q \left| S_m(k_q\Delta x) \right|^2}{d_i\kappa} \right]^2} \right.$$
$$\left. \pm \frac{1}{2}\left[d_i\kappa - \frac{1 - |\mathrm{SM}(k\Delta x)|^2 \sum_q \left| S_m(k_q\Delta x) \right|^2}{d_i\kappa} \right] \right). \tag{20}$$

It is instructive to compare this semi-discrete dispersion relation with the physical result ($\Delta x \to 0$), given by

$$\omega_{\mathrm{ph}} = \pm v_A k \left(\sqrt{1 + \frac{1}{4} d_i^2 k^2} \pm \frac{1}{2} d_i k \right). \tag{21}$$

In addition to the standard finite-difference modification of the wavenumber $k \to \kappa(k)$ (Appendix A), there are additional unphysical terms resulting from the Fourier representations of the shape functions and the smoothing operators. At this stage, the hybrid cancellation problem can be discerned: the presence of $d_i\kappa$ in the denominator of these unphysical terms may cause them to become arbitrarily large as $d_i k \to 0$.

To quantify these errors, it is necessary to compute the shape function terms $\sum_q \left| S_m(k_q\Delta x) \right|^2$, which involves analytically calculating the sum over aliases. Following Ref. [1],

$$\text{Nearest Grid Point (NGP, } m=0): \qquad \sum_q \left|S_0(k_q\Delta x)\right|^2 = 1, \tag{22}$$

$$\text{Cloud In Cell (CIC, } m=1): \qquad \sum_q \left|S_1(k_q\Delta x)\right|^2 = \frac{1}{3}\left[1+2\cos^2\left(\frac{1}{2}k\Delta x\right)\right], \tag{23}$$

$$\text{Quadratic Spline (QS, } m=2): \qquad \sum_q \left|S_2(k_q\Delta x)\right|^2 = \frac{1}{15}\left[2+11\cos^2\left(\frac{1}{2}k\Delta x\right)+2\cos^4\left(\frac{1}{2}k\Delta x\right)\right]. \tag{24}$$

The predicted dispersion relation from Eq. (20) is plotted as dashed lines in Fig. 1 for both left and right-hand polarized waves for the cases of NGP (blue), CIC (green), QS (red) without smoothing, and the case of QS with one pass of binomial smoothing (magenta) applied symmetrically to the field and moment quantities. The overplotted circles show the measured phase velocities from corresponding simulations using a 1D explicit electromagnetic hybrid algorithm, which verify the analytic result. Here, a small time-step is used to give negligible temporal truncation error and the wavelength of the perturbation is well resolved with 64 grid cells in each case, such that the spatial truncation errors are fixed ($k\Delta x = \pi/32$). The top horizontal axis gives the absolute size of the spatial cells in terms of the ion skin-depth, where $\Delta x/d_i \propto 1/kd_i$ for fixed $k\Delta x$.

For the short-wavelength limit ($d_i k \gg 1$), good agreement is found with Eq. (21) in each case for the right-hand polarized whistler ($\omega \propto k^2$) and the left-hand polarized ion cyclotron wave ($\omega \to \Omega_{ci}$). However, the correct long-wavelength limit ($\omega/kv_A \to 1$ as $kd_i \to 0$) is only recovered for the case of NGP without smoothing, for which the numerator is exactly zero for the unphysical terms in Eq. (20). For higher order shape functions, the phase-speed of the right (left) hand polarized waves is reduced (increased). This error increases as the width of the particle shape function is increased, and is further increased by the application of smoothing. The incorrect MHD-limit can be reached due to the inexact cancellation of the electric fields when combining the ion (19) and electron (15) momentum equations to find a total momentum equation, which is due to the convolutional smoothing of the shape function and grid smoothing operators in Eq. (19). The hybrid-PIC scheme is only spatially asymptotic preserving when $d_i/\Delta x \to 0$ for NGP.

4. Discussion

For linear problems, it is useful to estimate how large a value of $(\Delta x/d_i)$ can be taken for a given desired accuracy. To second order in the assumed small parameter $(k\Delta x) \ll 1$, $\kappa \approx k[1-(k\Delta x)^2/6]$, and

$$\frac{1-|SM(k\Delta x)|^2\sum_q\left|S_m(k_q\Delta x)\right|^2}{d_i\kappa} \approx C(k\Delta x)\left(\frac{\Delta x}{d_i}\right), \tag{25}$$

where the constant C depends on the order of the shape function and the amount of smoothing: $C=0$ for NGP, $C=1/6$ for CIC, $C=1/4$ for QS, and $C=3/4$ for QS with one pass of smoothing to the fields and moments.

The relative dispersion error due to the second-order finite-difference approximation, $\epsilon_{\text{FD}} = |\omega-\omega_{ph}|/\omega_{ph}$, can be computed by assuming $C=0$. For $kd_i \ll 1$, $\epsilon_{FD} \approx (k\Delta x)^2/6$. This can be compared with the estimated dispersion error contribution solely from the cancellation problem, ϵ_{CP}. Assuming $C \neq 0$, and then taking $(k\Delta x)^2 \ll (k\Delta x)(\Delta x/d_i) \sim \mathcal{O}(1)$, gives $\epsilon_{CP} \approx C(k\Delta x)(\Delta x/d_i)/2$. The cancellation error dominates the finite-difference error and determines the resolution requirements for $kd_i \ll 1$. The minimum mesh-spacing requirement to achieve a desired error ϵ for a specific wavenumber $(kd_i) \ll 1$ is therefore given by

$$\frac{\Delta x}{d_i} \lesssim \sqrt{\frac{2\epsilon}{C(kd_i)}}. \tag{26}$$

While the above results have been derived for parallel propagating waves with a uniform background density, similar dispersion errors due to the cancellation problem can be found for the case of fast magnetosonic waves propagating perpendicular to a background magnetic field. In Fig. 2, we give a dramatic non-linear numerical example of how such dispersion errors can lead to incorrect physics results. For this simulation, a cloud of debris ions with number density $n_d = (20n_b/\sqrt{\pi})\exp(-x^2/(15d_i)^2)$ and velocity $v_d = 5v_{Ab}\hat{\boldsymbol{x}}$ is released into a uniform background plasma with magnetic field $\boldsymbol{B}_0 = B_0\hat{\boldsymbol{z}}$, density n_b, Alfvén speed $v_{Ab} = B_0/\sqrt{m_b n_b \mu_0}$, cyclotron frequency $\Omega_{ci} = q_b B_0/m_b$ and skin-depth $d_i = v_{Ab}/\Omega_{ci}$. The ratio of debris ion charge and mass to background values is $q_d/q_b = 1$ and $m_d/m_b = 3$ respectively. The super-Alfvénic expansion of the debris ions excludes the background magnetic field to create a magnetic cavity, and couples with the background ions to create a perpendicular fast magnetosonic shock [15]. For higher-order shape functions, we observe that numerical dispersion errors are able to support the formation of unphysical solitons that are generated during non-linear steepening when the shock is formed. When followed for long time-scales, these unphysical solitons can detach and move ahead of the shock wave. Using either the NGP shape function or a sufficiently small $\Delta x/d_i \ll 1$ can remove these artifacts.

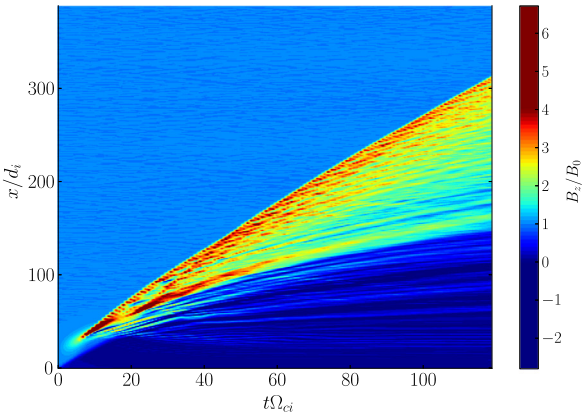

(a) Nearest Grid Point (NGP). $\Delta x/d_i = 1$.

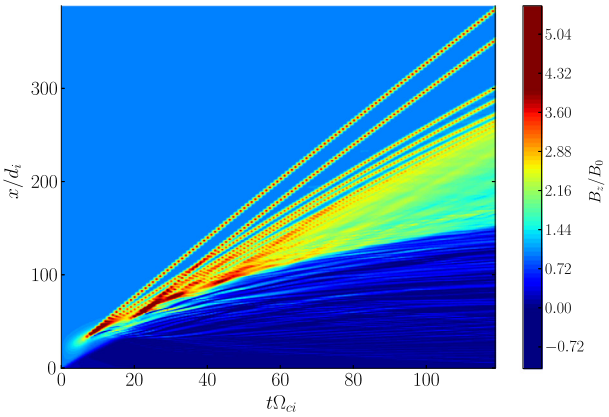

(b) Quadratic Spline (QS) with smoothing. $\Delta x/d_i = 1$.

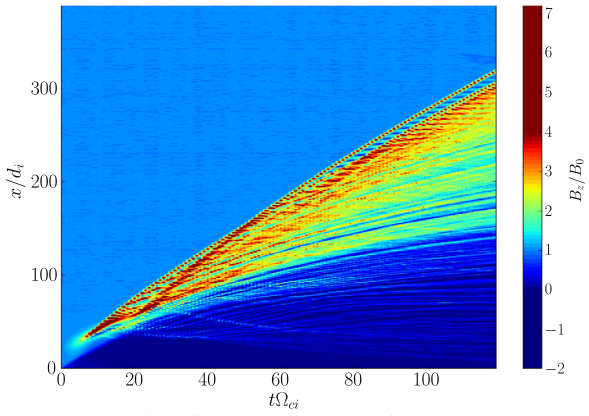

(c) Quadratic Spline (QS) with smoothing. $\Delta x/d_i = 0.5$

Fig. 2. a) Simulation with resolution $\Delta x/d_i = 1$ using NGP shows formation of perpendicular shock and magnetic cavity caused by the super-Alfvénic expansion of debris ions into a uniform magnetized background plasma. b) The same simulation, but with QS shape function and smoothing, gives unphysical solitons due to the interplay of numerical dispersion errors and non-linear steepening. c) At higher resolution $\Delta x/d_i = 0.5$, these solitons are reduced (although not completely removed at this resolution).

The form of cancellation errors in the dispersion relation of Eq. (20) appears similar to the cancellation problem found in electromagnetic gyrokinetic algorithms (see e.g. [16–18]). However, it is worth noting two differences. Firstly, the cancellation problem in hybrid-PIC is less restrictive than that in gyrokinetics, as it causes dispersion errors at the ion skin-depth scale rather than the electron skin-depth ($d_i/d_e = \sqrt{m_i/m_e} \gg 1$). Secondly, the cancellation problem occurs in gyrokinetics due to the choice of the parallel canonical momentum, $p_\parallel$, as a dependent variable, rather than $v_\parallel$. The $p_\parallel$ formulation is typically chosen for semi-implicit gyrokinetic schemes as the $v_\parallel$ formulation contains an implicit coupling. In fact, the gyrokinetic cancellation problem can be avoided entirely by solving the $v_\parallel$ formulation implicitly [19]. The hybrid-PIC cancellation problem is due to the different spatial discretization of ions (particles) and electrons (grid-based) and does not depend on the choice of time integration scheme. A possible alternate solution to the cancellation problem, which will be explored in future work, is to solve for the full (ion + electron) momentum equation on a spatial grid (e.g. [20]), and to use a particle kinetic ion discretization for only part of the ion distribution function (similar to a δF method).

CRediT authorship contribution statement

Adam Stanier: Conceptualization, Investigation, Software, Formal analysis, Writing, Vizualization. Luis Chacon: Conceptualization, Investigation, Software, Supervision, Funding acquisition. Ari Le: Investigation, Validation, Resources.

Declaration of competing interest

The authors declare that they have no known competing financial interests or personal relationships that could have appeared to influence the work reported in this paper.

Acknowledgements

A.S. thanks Dan Winske and David Burgess for useful discussions. This material is based upon work supported by the U.S. Department of Energy, Office of Science, Office of Applied Scientific Computing Research (ASCR). This research used resources provided by the Los Alamos National Laboratory Institutional Computing Program, which is supported by the U.S. Department of Energy National Nuclear Security Administration under Contract No. 89233218CNA000001. AL was supported by the Laboratory Directed Research and Development program of Los Alamos National Laboratory under project number 20200334ER.

Appendix A. Fourier transforms of relevant quantities

For a 1D periodic spatial domain of size L_x, with $x \in [0, L_x]$ and $k = 2\pi n/L_x$ for integer n, the continuum Fourier transform pair is given by

$$\widetilde{\chi}(k,t) = \int_0^{L_x} \chi(x,t) e^{-ikx} dx, \quad \chi(x,t) = \frac{1}{L_x} \sum_k \widetilde{\chi}(k,t) e^{ikx}. \tag{A.1}$$

On a uniform spatial grid of N_x cells, with X_g the cell positions, the discrete Fourier transform is defined as

$$\widetilde{F_g}(k,t) = \sum_{g=0}^{N_x-1} F_g(X_g,t) e^{-ikX_g} \Delta x, \quad F_g(X_g,t) = \frac{1}{L_x} \sum_k \widetilde{F_g}(k,t) e^{ikX_g}, \tag{A.2}$$

where the allowed $k = 2\pi n/L_x$ for $n \in [-N_x/2 + 1, N_x/2]$.

As an example, the Fourier transform of the smoothing operator is

$$\widetilde{\mathrm{SM}(F_g)} = \sum_{g=0}^{N_g-1} F_g e^{-ikX_g} \Delta x \left(\frac{e^{ik\Delta x} + 2 + e^{-ik\Delta x}}{4} \right) = \widetilde{F_g} \cos^2(k\Delta x/2), \tag{A.3}$$

and of the central differencing operator is

$$\widetilde{\frac{F_{g+1} - F_{g-1}}{2\Delta x}} = \sum_{g=0}^{N_g-1} F_g e^{-ikX_g} \Delta x \left(\frac{e^{ik\Delta x} - e^{-ik\Delta x}}{2\Delta x} \right) = \widetilde{F_g} ik \frac{\sin(k\Delta x)}{(k\Delta x)}. \tag{A.4}$$

As time is taken to be continuous, the time dependence is assumed of the form $e^{i\omega t}$ for variables defined both in the continuum and on the discrete spatial grid.

References

[1] C.K. Birdsall, A.B. Langdon, Plasma Physics via Computer Simulation, McGraw-Hill, New York, 1991.
[2] R.W. Hockney, J.W. Eastwood, Computer Simulation Using Particles, McGraw-Hill, New York, 1981.
[3] K.J. Bowers, B.J. Albright, L. Yin, W. Daughton, V. Roytershteyn, B. Bergen, T.J.T. Kwan, J. Phys. Conf. Ser. 180 (1) (2009) 012055, https://doi.org/10.1088/1742-6596/180/1/012055.
[4] W.M. Nevins, G.W. Hammett, A.M. Dimits, W. Dorland, D.E. Shumaker, Discrete particle noise in particle-in-cell simulations of plasma microturbulence, Phys. Plasmas 12 (12) (2005) 122305, https://doi.org/10.1063/1.2118729.
[5] P.W. Rambo, Finite-grid instability in quasineutral hybrid simulations, J. Comput. Phys. 118 (1995) 152–158, https://doi.org/10.1006/jcph.1995.1086.
[6] J. Byers, B. Cohen, W. Condit, J. Hanson, Hybrid simulations of quasineutral phenomena in magnetized plasma, J. Comput. Phys. 27 (3) (1978) 363–396, https://doi.org/10.1016/0021-9991(78)90016-5.
[7] D.W. Hewett, C.W. Nielson, A multidimensional quasineutral plasma simulation model, J. Comput. Phys. 29 (2) (1978) 219–236, https://doi.org/10.1016/0021-9991(78)90153-5.
[8] D. Winske, L. Yin, N. Omidi, H. Karimabadi, K. Quest, Hybrid simulation codes: past, present and future - a tutorial, in: J. Büchner, C. Dum, M. Scholer (Eds.), Space Plasma Simulation, in: Lecture Notes in Physics, vol. 615, Springer-Verlag, Berlin, 2003, pp. 136–165.
[9] A. Stanier, L. Chacon, G. Chen, A fully implicit, conservative, non-linear, electromagnetic hybrid particle-ion/fluid-electron algorithm, J. Comput. Phys. 376 (2019) 597–616.
[10] D. Winske, Hybrid simulation codes with application to shocks and upstream waves, Space Sci. Rev. 42 (1–2) (1985) 53–66.
[11] I.T. Chapman, J.P. Graves, M. Lennholm, J. Faustin, E. Lerche, T. Johnson, S. Tholerus, The merits of ion cyclotron resonance heating schemes for sawtooth control in tokamak plasmas, J. Plasma Phys. 81 (6) (2015) 365810601, https://doi.org/10.1017/S0022377815000987.
[12] H. Karimabadi, V. Roytershteyn, H.X. Vu, Y.A. Omelchenko, J. Scudder, W. Daughton, A. Dimmock, K. Nykyri, M. Wan, D. Sibeck, M. Tatineni, A. Majumdar, B. Loring, B. Geveci, The link between shocks, turbulence, and magnetic reconnection in collisionless plasmas, Phys. Plasmas 21 (6) (2014) 062308, https://doi.org/10.1063/1.4882875.
[13] A. Stanier, W. Daughton, L. Chacón, H. Karimabadi, J. Ng, Y.-M. Huang, A. Hakim, A. Bhattacharjee, Role of ion kinetic physics in the interaction of magnetic flux ropes, Phys. Rev. Lett. 115 (17) (2015) 175004, https://doi.org/10.1103/PhysRevLett.115.175004.
[14] A. Le, V. Roytershteyn, H. Karimabadi, A. Stanier, L. Chacon, K. Schneider, Wavelet methods for studying the onset of strong plasma turbulence, Phys. Plasmas 25 (12) (2018) 122310, https://doi.org/10.1063/1.5062853.

[15] D. Winske, S.P. Gary, Hybrid simulations of debris-ambient ion interactions in astrophysical explosions, J. Geophys. Res. Space Phys. 112 (A10) (2007) A10303, https://doi.org/10.1029/2007JA012276.
[16] J.C. Cummings, Gyrokinetic simulation of finite-beta and self-generated sheared-flow effects on pressure-gradient-driven instabilities, 1996.
[17] A. Mishchenko, A. Bottino, R. Hatzky, E. Sonnendrücker, R. Kleiber, A. Könies, Mitigation of the cancellation problem in the gyrokinetic particle-in-cell simulations of global electromagnetic modes, Phys. Plasmas 24 (8) (2017) 081206.
[18] N. Mandell, A. Hakim, G. Hammett, M. Francisquez, Electromagnetic full-f gyrokinetics in the tokamak edge with discontinuous Galerkin methods, arXiv preprint, arXiv:1908.05653, 2019.
[19] B. Sturdevant, S.-H. Ku, C. Chang, R. Hager, L. Chacon, G. Chen, A fully implicit particle-in-cell method for gyrokinetic electromagnetic modes in xgc, Bull. Am. Phys. Soc. (2019).
[20] T. Amano, A generalized quasi-neutral fluid-particle hybrid plasma model and its application to energetic-particle-magnetohydrodynamics hybrid simulation, J. Comput. Phys. 366 (2018) 366–385, https://doi.org/10.1016/j.jcp.2018.04.020, arXiv:1804.03586.